Impact of Zn-doped Manganese Oxide Nanoparticles on Structural and Optical Properties

V. Yadav, R. Shukla*, K. S. Sharma

Department of Physics, IIS, Jaipur-302020, India

Abstract

In the present work, the structural and optical properties of pure and zinc-doped manganese oxide nanoparticles prepared by the sol-gel method have been studied for doping concentrations of 5, 10, and 15 %. The XRD patterns reveal that the cubic phase of pure manganese oxide nanoparticles is changed to tetragonal on doping with Zn. The surface morphology of pure and Zn doped manganese oxide nanoparticles has been studied by Scanning Electron Microscopy (SEM), which reveals appreciable changes in size and shape of the nanoparticles as the doping level of Zn is increased. The optical properties studied by UV-Visible spectroscopy further reveal that the energy band gap increases with a decrease in the size of nanoparticles.

1. Introduction

Recently metal oxide nanoparticles (NPs) have been of much interest because of their unique optical, electronic, and magnetic properties, which often differ substantially from the bulk. Transition metal oxide NPs, form a wide class of useful materials because of their fascinating electronic and magnetic properties. Transition metal oxide NPs have numerous applications as catalysts, sensors, superconductors, magnetic resonance imaging (MRI) and sun-based cells, and adsorbents [1]. As an important functional metal oxide, manganese oxide in NPs form is one of the most attractive inorganic materials because of its physical and chemical properties and wide range of applications such as in catalysis, ion exchange, molecular adsorption, biosensors, and particularly in energy storage [2-4].

Several forms of manganese oxides are possible due to various oxidation states shown by manganese, viz. Mn (II, III, IV). Manganese dioxide is the most widely used cathode material in primary and secondary batteries due to its high capacity and low toxicity [5]. The most commonly known manganese oxides, MnO, Mn_2O_3, and Mn_3O_4 have a wide range of applications in catalysis and battery technologies. MnO_2 crystals have been used in the past for water treatment and biosensors development. Polymorphs

---

* *Corresponding author*: rimshu21@gmail.com

of Mn_2O_3 have been used as catalysts for removing carbon monoxide and nitrogen oxide from the waste gas. Researchers have shown considerable interest in the last few years in lithium intercalated Mn_2O_3, which is used as an electrode material for rechargeable lithium batteries [6].

It is also used to prepare soft magnetic materials, such as manganese, and zinc ferrites, which are useful for constructing magnetic cores transformers used in power supplies. It is one of the raw materials used to manufacture professional-grade ferrites [7]. Zn is an essential trace element for the human system, without which many enzymes, such as carbonic anhydrase, carboxypeptidase, and alcohol dehydrogenase, become inactive. Zn doping in manganese oxide NPs may change their structural, optical, and electronic properties, so the objectives of the present study are to examine the effect of Zn on the crystal structure of manganese oxide nanoparticles.

Doping of a metal oxide with low valence positive ions results in the breakdown of the regular symmetry of the material, which results in a change in the electronic potential at the sites of the substituted atoms. Hence, the material's electronic properties are considerably changed [8].

Some results have been reported in the literature on the Mn-doped zinc oxide NPs for different applications [9], but there is very less work has been done on the Zn-doped manganese oxide NPs; the present study will provide information about the structural properties of Zn-doped manganese oxide NPs at different levels of doping.

The scope of the present work was to synthesize and investigate various properties of pure and zinc (5 %, 10 %, and 15 %) doped manganese oxide NPs. The prepared samples' structural, morphological, and optical properties have been investigated using X-ray diffraction (XRD) analysis, scanning electron microscopy (SEM), and UV-Visible spectroscopy, respectively.

2. Experiment

In the present research, the pure and zinc doped manganese oxide nanoparticles (NPs) were synthesized by the Sol-Gel Method, using manganese acetate tetrahydrate and zinc acetate dihydrate as a precursor and sodium hydroxide (NaOH) as a stabilizing agent. The materials used to synthesize NPs were analytical grade reagents purchased from Merck INDIA company with 99.5 % purity.

The instrument used in this experiment for the preparation of NPs by the Sol-Gel method is a generic magnetic stirrer with a hot plate -MH 2ltr with a Teflon magnet.

For the preparation of samples of NPs of materials to be studied, the procedure and protocol described by Uche [5], also called the Sol-Gel method, is used in the present work. This process has been successfully used earlier in several types of research, for example, by Iqbal *et al.* [10] for the formation of NPs of silver oxide, Zinc oxide, Titanium oxide, etc.

In the present research, the pure and zinc doped manganese oxide nanoparticles were synthesized by the above-mentioned Sol-Gel method, using manganese acetate

tetrahydrate and zinc acetate dihydrate as a precursor and sodium hydroxide (NaOH) as a stabilizing agent.

To synthesize pure MnO NPs, manganese acetate tetrahydrate (2.00 g) and oxalic acid (6.00 g) were separately dissolved in 200 mL ethanol each. The manganese acetate tetrahydrate solution was stirred continuously for 30 min while maintaining it at 40 °C. Then the oxalic acid solution was added to the warm solution of manganese acetate tetrahydrate, which quickly formed a white precipitate, indicating the formation of pure MnO. Finally, the precipitate was washed with ethanol to remove impurities and then filtered. After that, the precipitate was dried in the hot air oven overnight while maintaining it at the temperature of 100 °C. The synthesized samples were annealed at 450 °C in a muffle furnace to improve the crystallinity. After annealing, the color of the decomposed sample was changed from white to black. The same procedure was adopted for preparing Zn-doped manganese oxide samples by adding different concentrations of zinc acetate dihydrate to manganese acetate tetrahydrate solutions.

The crystal structure of the sample was investigated using a Panalytical Empyrean diffractometer equipped with 1.54Å Cu-kα radiation in the 2θ range of 20-80° at room temperature. The surface analysis of the sample was investigated using a (Zeiss EVO 18) and (JEOL JSM 7610F) scanning electron microscope (SEM). Perkin Elmer (Lambda 750) UV-Visible spectrometer was used to investigate the optical properties of the samples. Perkin Elmer variation 7000 FT-IR was used to investigate various functional groups on the surface of synthesized materials.

3. Results and Discussion

3.1. *XRD analysis*

To determine the size of crystallite size and their structure, XRD was done for all the prepared samples. The XRD patterns obtained for pure and zinc doped manganese oxide nanoparticles for doping concentrations (5, 10, and 15 %), annealed at 450 °C, are shown in Fig. 1. All the obtained peaks and their respective planes for pure Mn_2O_3 are well-matched with the JCPDS (00-41-1442) data. From this comparison, we obtain the crystal structure of manganese oxide, which has a Mn_2O_3 phase and cubic lattice. The average crystallite size (D) of pure manganese oxide was found to be 17 nm using Debye-Scherrer's formula [11]

$$D = 0.9\lambda/\beta\cos\theta \qquad (1)$$

Where λ is the wavelength of X-ray used (which is 0.15406 nm in the present case), β is the full width at half maximum (FWHM) of the peaks obtained in XRD pattern and θ is the angle of diffraction. X-ray spectra for pure Mn_2O_3 shown in Fig. 1 has similarity to that reported by [12].
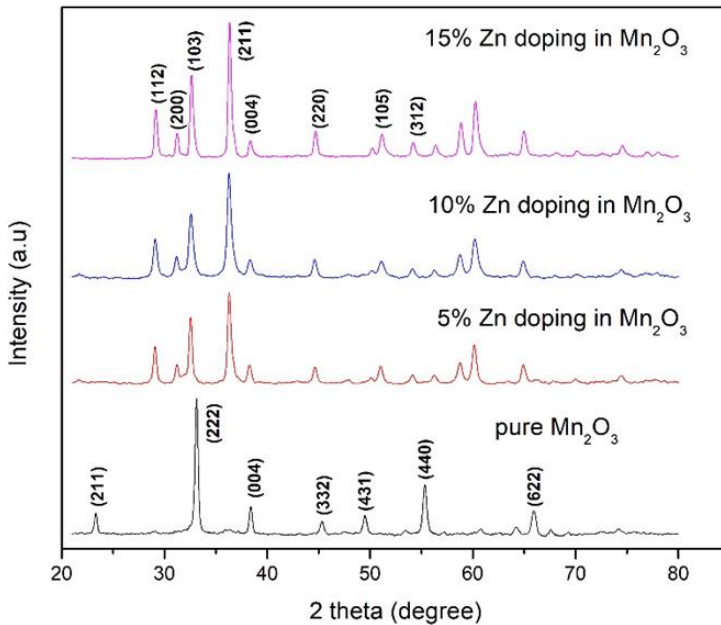
Fig. 1. XRD pattern for pure and Zn (5, 10, and 15 %) doped manganese oxide NPs.

In the XRD patterns of Zn doped manganese oxide, all the peaks are well-matched with the JCPDS cards (00-024-1133 and 01-077-0470) data. From this comparison, it is also found that on doping with Zn, the phase of manganese oxide changes from Mn_2O_3 (cubic) to $ZnMn_2O_4$ (tetragonal structure). From the XRD pattern of Zn doped manganese oxide, the reflection peaks are obtained at the same position for three levels of doping but their intensity increases as the doping concentration of Zn is increased. The reason for that is the higher reflectance of Zn ions as compared to Mn ions. The crystallite size for the Zn (5, 10, and 15 %) doping in manganese oxide is found to be 15, 11, and 20 nm respectively (Table 1). So the crystallite size of Zn doped manganese oxide decreases as the level of Zn is increased from 5% to 10% due to quantum confinement in nanomaterials [13]. For the higher doping value of Zn, Mn^{+3} (0.58 Å) states are found to be present, which have smaller ionic radii than Zn^{+2} (0.74 Å), and therefore as we increase the doping level of Zn from 10 to 15%, the crystallite size increases [14], showing that the size of crystallites in a material depends on the type of ions and ionic states present in the material.

3.2. *Surface analysis*
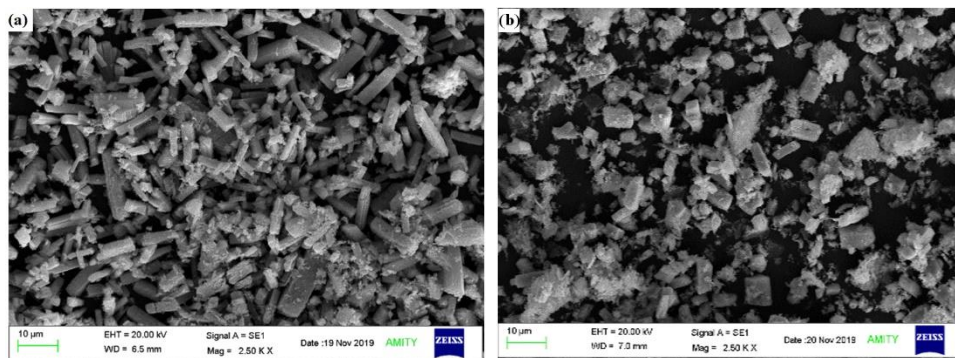
Fig. 2. (a) SEM image for pure Mn_2O_3, (b) SEM image for 5 % Zn doping in Mn_2O_3.
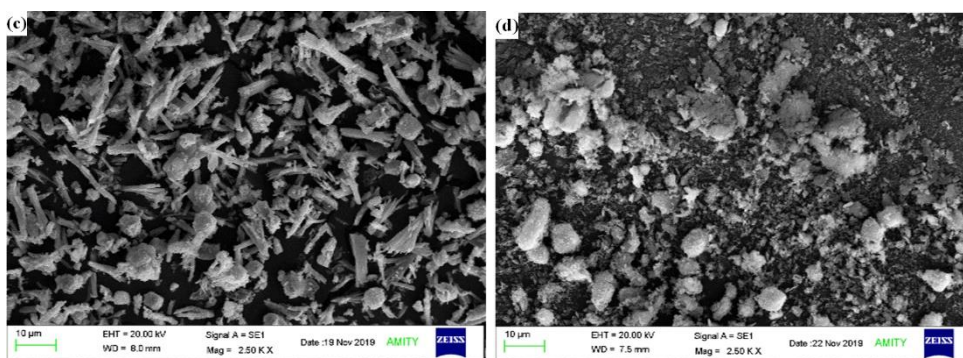
Fig. 2. (c) SEM image for 10 % Zn doping in Mn_2O_3, (d) SEM image for 15 % Zn doping in Mn_2O_3.

Fig. 2 (a) shows the SEM image of Mn_2O_3 NPs. It shows the presence of rod and rectangle-shaped particles. The particle size obtained from SEM is between 800-1200 nm. Figs. 2. (b), (c), and (d) show the SEM images for Zn (5, 10, and 15 %) doped manganese oxide NPs where the structural deformation from nanorods to a mixture of nanorods and NPs can be noticed. So, after the doping of Zn, particle shape changed from nanorods to NPs. From the SEM images, the particle size for 5, 10 and 15 % Zn doping in manganese oxide is found to be in the range of 400-600 nm, 80-400 nm, and 600-800 nm, respectively. So as we increase the Zn doping percentage from 5 % to 10 %, the particle size is decreased, and particle size increases on increasing Zn concentration from 10 to 15 %. Thus, particle size and morphology strongly depend on the doping level of Zn. Further, the particle size obtained from the SEM micrographs is much greater than the XRD results, which may be because of the aggregation of smaller particles while preparing SEM samples. So the morphology of manganese oxide NPs is changed after the Zn doping, which conforms with the previously reported literature [15-17].

3.3. *Optical properties*

Energy bandgap

The optical properties of the synthesized samples were determined by using UV-Visible spectroscopy.
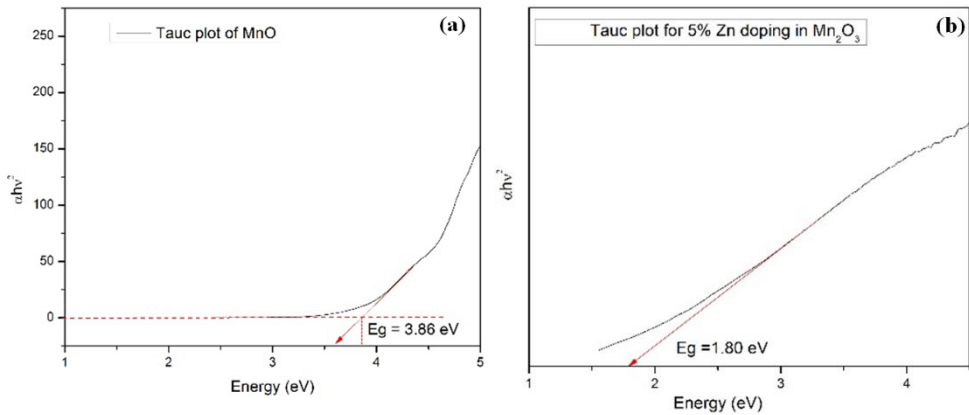
Fig. 3. (a) Tauc plot for pure Mn_2O_3, (b) Tauc plot for 5 % Zn doping in Mn_2O_3.
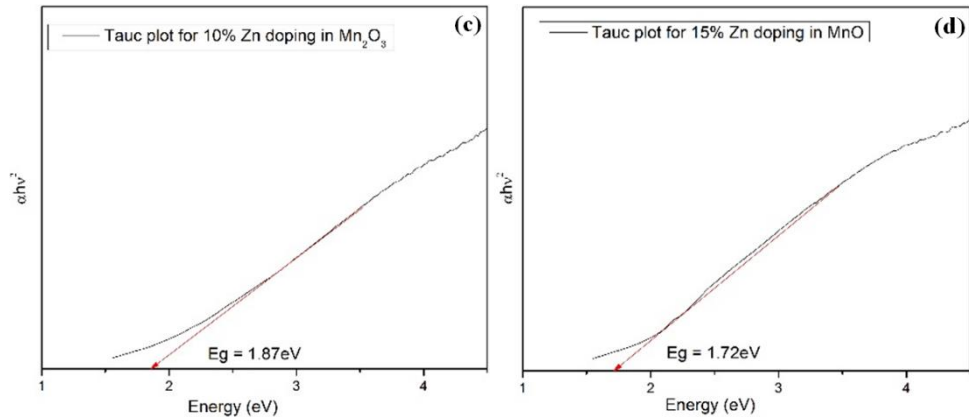
Fig. 3. (c) Tauc for 10 % Zn doping in Mn_2O_3, (d) Tauc plot for 15 % Zn doping in Mn_2O_3.

Figs. 3(a) to 3(d) show the Tauc plots for pure and Zn (5, 10 and 15 %) doped manganese oxide NPs. The Tauc plots are the diagram showing a variation of the quantity ($\alpha h\nu^2$), with a photon energy of the incident light.

The optical band gap can be calculated from the Tauc plot using the relation,

$$Eg = 1240/\lambda \ \underline{\hspace{4cm}} \tag{2}$$

Where λ is the absorption wavelength, the value of the energy bandgap for pure and Zn (5, 10, and 15 %) doped in manganese oxide samples were found to be 3.86, 1.80, 1.87, and

1.72 eV respectively (Table 1). So the bandgap of Mn_2O_3 decreases on doping it with 5 % Zn and then on increasing doping level of Zn from 5 to 10 % the bandgap increases. For higher doping concentration (15 %) of Zn, the bandgap decreases again from 1.87 eV to 1.72 eV as observed from XRD and SEM analysis, particle size increases for 15 % doping [18,19]. So this is in agreement with above results.

3.4. *Absorbance*
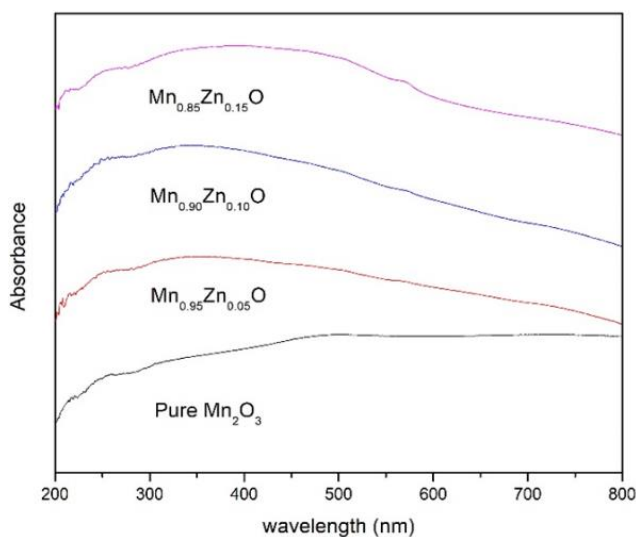
Fig. 4. Absorption spectra for pure and Zn (5, 10, and 15 %) doped Mn_2O_3 nanoparticles.

The absorption peaks for pure and Zn (5, 10, and 15 %) doped manganese oxide NPs are found to be at wavelengths 501, 350, 343, and 387 nm, respectively, as shown in Fig. 4 (Table 1) [20].

Table 1. Comparison of the Energy gap, absorption wavelength, and crystallite size of pure and Zn doped manganese oxide NPs.

Samples	Absorption Wavelength (nm)	Bandgap (eV)	Crystallite size from XRD (nm)
Pure Mn_2O_3	501	3.86	17
5% Zn doping in MnO	350	1.80	15
10% Zn doping in MnO	343	1.87	11
15% Zn doping in MnO	387	1.72	20

3.5. *Transmittance*

Transmittance for pure and Zn (5, 10, and 15 %) doped manganese oxide NPs is found to be at 17, 12, 15, and 19 %, respectively, which shows that on adding Zn to Mn_2O_3, transmittance first decreases and then increases, its value for 15 % Zn doped Mn_2O_3 being greater than pure Mn_2O_3 (Fig. 5).
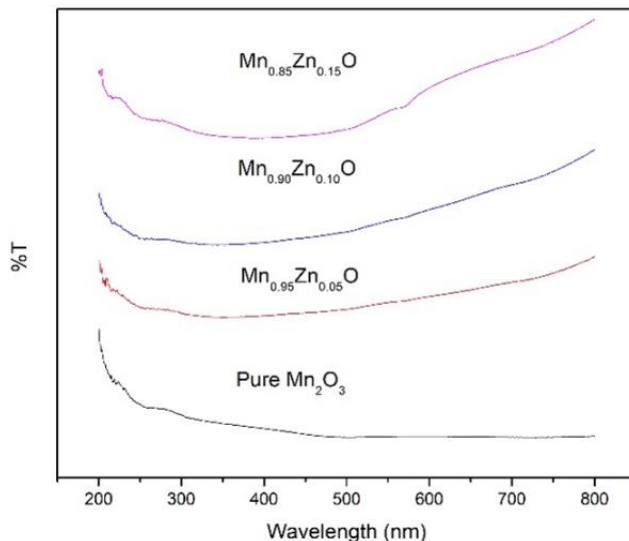
Fig. 5. Transmittance spectra for pure and Zn (5%, 10%, and 15%) doped Mn_2O_3 nanoparticles.

3.6. *Fourier transform infrared spectroscopy*

Fig. 6. shows the IR spectra for pure and Zn (5, 10, and 15 %) doped manganese oxide NPs. The percentage transmittance of the radiations for the samples was recorded in the range of 400 to 4000 cm^{-1}. The absorption peaks are observed to lie between 1400 and 1650 cm^{-1}, corresponding to the asymmetric and symmetric stretching of the carboxyl group (C=O) due to absorbed carbon dioxide on the surface of the material. The absorption peak around 2323 cm^{-1} arises due to O-H stretching due to the absorption of water by nanoparticles during the powder fabrication. Further, we observe very strong bands at 449, 484, and 613 cm^{-1} due to the Mn-O and (Mn-Zn)-O stretching modes. Hence, the appearance of M-O or M-O-M (M=Mn and Zn) and O-H is confirmed from the FTIR band of Mn_2O_3 and $Zn-Mn_2O_3$ NPs. The FTIR spectra observed in this study are consistent with reported literature [21-23]. After doping of Zn in manganese oxide NPs, bands are shifted towards higher wavenumber.
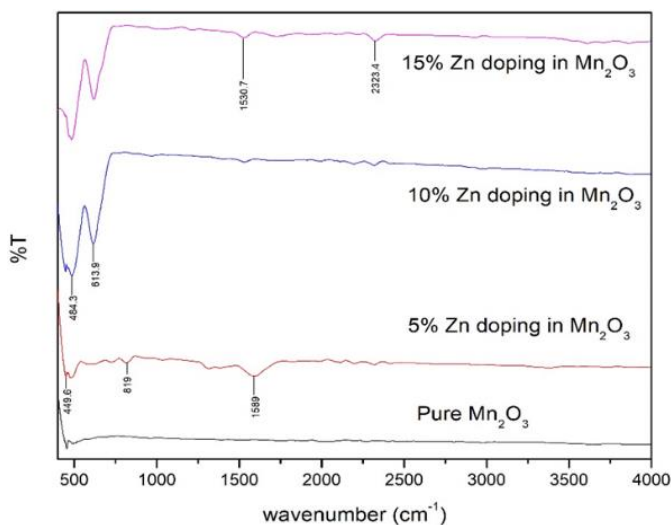
Fig. 6. IR spectra of pure and Zn (5, 10, and 15 %) doped manganese oxide.

4. Conclusion

Pure manganese oxide and Zn-doped (5, 10 and 15 %) manganese oxide NPs were successfully synthesized by the Sol-gel method. XRD results show a change in the crystal structure of Mn_2O_3 from cubic to tetragonal when Zn is doped in manganese oxide. The crystallite size decreases with an increase in doping percentage. The energy gap of Mn_2O_3 calculated using UV-VIS spectroscopy shows a decrease in bandgap from 3.86 to 1.80 eV after doping with Zn and then increases from 1.80 to 1.87 eV on increasing doping percentage from 5 % to 10 %. SEM micrographs indicate changes in the shape change of NPs on increasing doping level of Zn. The samples of pure manganese oxide and Zn (5, 10 and 15 %) doped manganese oxide NPs exhibit absorption edges to occur at 501, 350, 343, and 387 nm, respectively. The bandgap is decreased as the doping concentration is increased, and the absorption wavelength shifts towards the lower values on doping Mn_2O_3 with Zn, but for higher doping levels, it is found to increase.

References

1. P. Z. Si, D. Li, C. J. Choi, Y. B. Li, D. Y Geng and Z. D. Zhang, Solid State Commun. **142**, 723, (2007). https://doi.org/10.1016/j.ssc.2007.04.029
2. J. Park, E. Kang, C. J. Bae, J. –G. Park, H. –J. Noh, et al. J. Phys. Chem. B **108**, 13594 (2004). https://doi.org/10.1021/jp048229e
3. S. Lei, K. Tang, Z. Fang, and J. Sheng, J. Nanoparticle Res. **9**, 833 (2007). https://doi.org/10.1007/s11051-006-9131-4
4. R. Ramachandran, J. Mater. Sci.: Mater. Electron. **13**, 257 (2002). https://doi.org/10.1023/A:1015534901166
5. D. Okpala and V. Uche, Pelagia Res. Libr. Adv. Appl. Sci. Res. **4**, 506 (2013).
6. T. Iqbal, S. Tufail, and S. Ghazal, Int. J. Nanosci. Nanotechnol. **13**, 19 (2017).

7. X. Li, L. Zhou, J. Gao, H. Miao, H. Zhang, and J. Xuc, Powder Technol. **190**, 324 (2009). https://doi.org/10.1016/j.powtec.2008.08.010
8. M. Wang, L. Chen J. Zhou, L. Xu, X. Li, L. Li, and X. Li., J. Mater. Sci. **54** 483 (2019). https://doi.org/10.1007/s10853-018-2840-0
9. S. Mohsin, F. Naila, and S. Muhammad, Physica B: Phys. Condensed Matter **412,** 504 (2020).
10. P. Scherrer, The Eur. Digital Math. Libr. **1918**, 98 (1918).
11. B. D. Cullity, and J. W. Weymouth, Am. J. Phys. **25**, 394 (1957). https://doi.org/10.1119/1.1934486
12. S. Paramvir, R. Jain et. al., Advances in Nanotechnology, 1st Edition, Chapter 9 (Z Bartul and J Trenor, 2015).
13. K. S. Pugazhvadivu, K. Ramachandran, and K. Tamilarasan, Phys. Procedia **49**, 205 (2013). https://doi.org/10.1016/j.phpro.2013.10.028
14. W. K. Ababay, A. W. Delele, and H. G. Nigus, Appl. Sci. **452**, 4746, (2021).
15. O. Bayram, M. E. Ertargin, E. Iqman, H. Guney, and O. Simsek, J. Mater. Sci.: Mater. Electron. **10854**, 8980 (2018). https://doi.org/10.1007/s10854-018-8980-9
16. R. Poonguzhali, N. Shanmugam, R. Gobi, A. Senthilkumar, R. Shanmugam, and K. Sathishkumar, RSC Adv. **5**, 45407 (2015). https://doi.org/10.1039/C5RA01326G
17. A. Jha, R. Thapa, K. K. Chattopadhyay, Mater. Res. Bull. **47**, 813 (2012). https://doi.org/10.1016/j.materresbull.2011.11.057
18. S. dawadi, G. Aakash, K. Manita, B. Budhathoki, G. Lamichhane, et al., Ind. Acad. Sci. **277**, 1 (2020). https://doi.org/10.1007/s12034-020-02247-8
19. M. S. Roxy, A. Ananthu, and V. B. Sumithranand, Int. J. Sci. Res. Sci. Eng. Tech. **8**, 134 (2021). https://doi.org/10.32628/IJSRSET218225
20. S. Karpagavalli, S. J. K. Vethanathan, S. Perumal, D. P. Koilpillai, and A. Suganthi, J. Appl. Phys. **4861**, 34 (2017). https://doi.org/10.9790/4861-17002013442
21. A. V. Olmos, R. Redon, M. E. Mata-Zamora, F. Morales-Leal, A. L. Fernandez-Osorio, et. al., J. Colloid Interface Sci. **291**, 175 (2005). https://doi.org/10.1016/j.jcis.2005.05.005
22. T. M. Francis, P. R. Lichty, and A. W. Weimer, Chem. Eng. Sci. **65**, 3709 (2010). https://doi.org/10.1016/j.ces.2010.03.002
23. M. Suriyavathana and K. Ramalingam, Int. J. Chem. Tech. Res. **8**, 466 (2015).